final state of scalarization, then the coexisting KN black holes must have lower angular momentum than the initial unstable ones. As the spin-induced tachyonic instability is suppressed at lower spin, the coexisting KN black holes could be stabilized, provided the angular momentum loss is sufficiently large. Electromagnetic radiation may play an important role in achieving this loss, as electromagnetic wave emission is significantly more efficient than gravitational wave emission in radiating energy and angular momentum when the black hole charge is comparable to its mass.

Furthermore, in contrast to the EsGB theories where spin-induced scalarized black holes are entropically favored, we found that, in the EMS models, KN black holes possess higher entropy in the coexisting region. Although entropic preference does not necessarily align with dynamical stability due to dissipative processes, this observation suggests that spin-induced scalarized KN black holes might be metastable and could eventually decay into stable KN black holes.

To better understand these phenomena, future investigations should address two open questions: (1) the linear stability of spin-induced scalarized KN black holes against radial and nonaxisymmetric perturbations, and (2) the nonlinear dynamical evolution of spin-induced scalarization. Resolving these issues will clarify whether spin-induced scalarized KN black holes represent a transient phase in black hole evolution or a persistent configuration, with implications for gravitational wave astronomy and high-energy astrophysics.

ACKNOWLEDGMENTS

We are grateful to Yiqian Chen for useful discussions and valuable comments. This work is supported in part by NSFC (Grant Nos. 12275183, 12275184, 12347133 and 12250410250).

Appendix A: Convergence Tests

To assess the numerical accuracy of our scalarized black hole solutions, we perform convergence tests by evaluating the absence of conical singularities and verifying the Smarr relation. Specifically, we define the conical singularity error as $E_C = \max_{-1\leq x\leq 1} |F_1(x,0) - F_2(x,0)|$ and the Smarr relation error as $E_S = |1 - (2T_H S + 2\Omega_H J + \Phi Q)/M|$. Figs. 4 and 5 show logarithmic plots of these errors as functions of N_x (with $N_\theta = 11$) and N_θ (with $N_x = 40$), respectively. The left, middle and right columns correspond to scalarized black holes near the bifurcation line, between the bifurcation and critical lines and on the critical line, respectively. These results demonstrate exponential

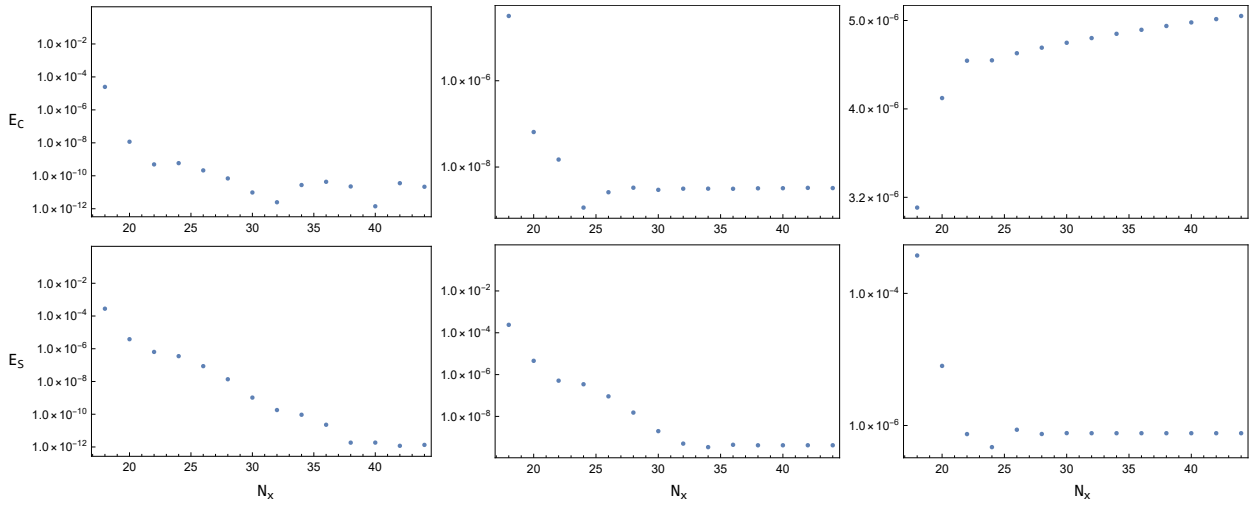

FIG. 4. Logarithmic plots of the conical singularity error E_C (**Upper Row**) and the Smarr relation error E_S (**Lower Row**) as functions of the radial resolution N_x, with fixed angular resolution $N_\theta = 11$, for scalarized black holes near the bifurcation line (**Left Column**), between the bifurcation and critical lines (**Middle Column**) and on the critical line (**Right Column**).

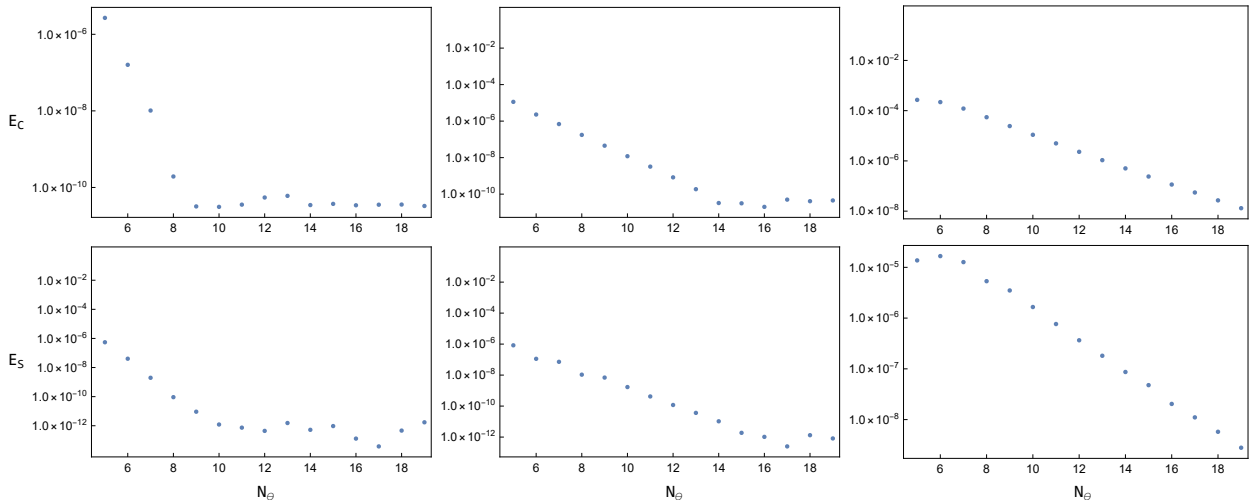

FIG. 5. Logarithmic plots of the conical singularity error E_C (**Upper Row**) and the Smarr relation error E_S (**Lower Row**) as functions of the angular resolution N_θ, with fixed radial resolution $N_x = 40$, for scalarized black holes near the bifurcation line (**Left Column**), between the bifurcation and critical lines (**Middle Column**) and on the critical line (**Right Column**).

convergence of the numerical errors, followed by round-off plateaus[1]. Notably, the round-off plateau for E_S typically occurs later than for E_C. In particular, for the scalarized black hole near the bifurcation line, E_S reaches the plateau at $N_x = 40$ and $N_\theta = 11$. Based on these findings, we

[1] In the upper-right panel of Fig. 4, the conical singularity error E_C for the critical scalarized black hole has already reached a plateau within the plotted range of the resolution N_x.

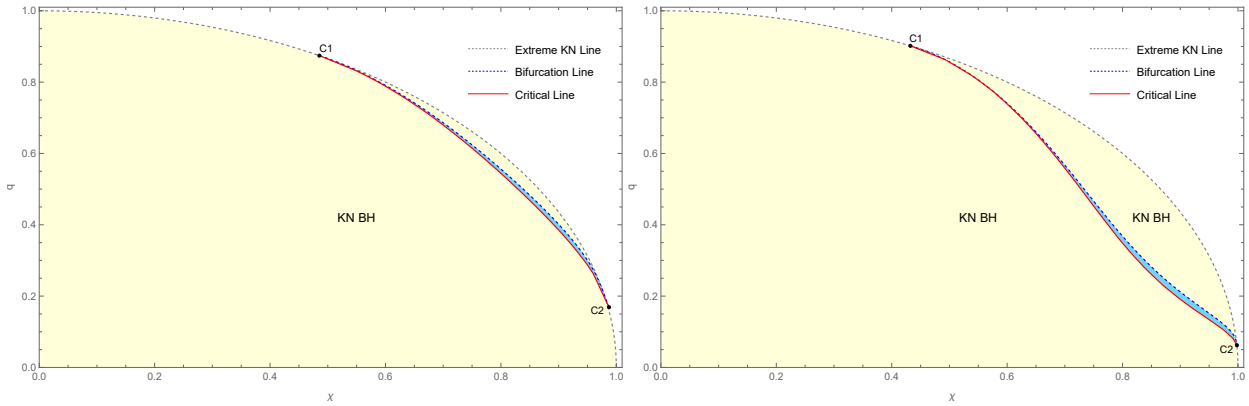

FIG. 6. Domain of existence for spin-induced scalarized KN black holes in the (χ, q) plane with the quadratic coupling function $f(\phi) = 1 + \alpha\phi^2$. **Left Panel:** $\alpha = -100$. **Right Panel:** $\alpha = -1000$.

employ spectral methods with resolutions $N_x = 40$ and $N_\theta = 11$ to solve the partial differential equations, ensuring both numerical precision and computational efficiency.

Appendix B: Quadratic Coupling Function

In this appendix, we consider the quadratic coupling function $f(\phi) = 1 + \alpha\phi^2$. The domain of existence for spin-induced scalarized black hole solutions in this case closely resembles that obtained with the exponential coupling function, indicating that the specific form of the coupling function does not significantly affect the structure of scalarized black hole solutions. As shown in Sec. III, the scalar field contributes only a small fraction to the total energy and therefore plays a limited role in determining the background geometry. The similarity in the existence domains for different coupling functions may be attributed to the suppressed nonlinear effects of the scalar field.

[1] B. P. Abbott et al. Observation of Gravitational Waves from a Binary Black Hole Merger. *Phys. Rev. Lett.*, 116(6):061102, 2016. arXiv:1602.03837, doi:10.1103/PhysRevLett.116.061102. I

[2] Kazunori Akiyama et al. First M87 Event Horizon Telescope Results. I. The Shadow of the Supermassive Black Hole. *Astrophys. J. Lett.*, 875:L1, 2019. arXiv:1906.11238, doi:10.3847/2041-8213/ab0ec7. I

[3] Kazunori Akiyama et al. First M87 Event Horizon Telescope Results. II. Array and Instrumentation. *Astrophys. J. Lett.*, 875(1):L2, 2019. arXiv:1906.11239, doi:10.3847/2041-8213/ab0c96.